

Tuning contact angles of aqueous droplets on hydrophilic and hydrophobic surfaces by surfactants

Fabio Staniscia, Horacio V. Guzman, and Matej Kanduč*

Department of Theoretical Physics, Jožef Stefan Institute, SI-1000 Ljubljana, Slovenia

E-mail: matej.kanduc@ijs.si

Abstract

Adsorption of small amphiphilic molecules occurs in various biological and technological processes, sometimes desired, the other times unwanted (*e.g.*, contamination). Surface-active molecules preferentially bind to interfaces and affect their wetting properties. We study the adsorption of short-chained alcohols (simple surfactants) to the water–vapor interface and solid surfaces of various polarities using molecular dynamics simulations. The analysis enables us to establish a theoretical expression for the adsorption coefficient, which exponentially scales with the molecular surface area and the surface wetting coefficient, and which is in good agreement with the simulation results. The competition of the adsorptions to both interfaces of a sessile droplet alters its contact angle in a nontrivial way. The influence of surfactants is strongest on very hydrophilic and very hydrophobic surfaces, whereas droplets on surfaces of moderate hydrophilicity are much less affected.

KEYWORDS: *adsorption, solvation, wetting, contact angle, molecular dynamics simulation*

1. INTRODUCTION

Adsorption of dissolved molecules from an aqueous phase onto interfaces with air and solids is a ubiquitous phenomenon in natural and technological processes. For instance, the adsorption of organic material (*e.g.*, microorganisms and pollen) plays a prominent role in several aspects of atmospheric and oceanic environments.^{1–4} Adsorption is essential in many applications, ranging from detergency, printing, surface catalysis, dialysis, filtration⁵ to petrochemical processes⁶ and removal of water pollutants.⁷ Yet, adsorption is a process often challenging to predict and control. Uncontrolled adsorption contributes to surface contamination, biofouling (*i.e.*, unwanted bacterial adhesion), loss of product to vessel surfaces, clogging of small constrictions in coronary stents^{8,9} or microfluidic devices,¹⁰ and deterioration of biosensors.¹¹

It is known that many small molecules and proteins tend to adsorb better onto hydrophobic surfaces, while hydrophilic surfaces are generally more resistant to adsorption,^{12–14} making them suitable self-cleaning materials against biofouling.⁹ Using water contact angle as a proxy for the hydrophobicity of the surface became attractive, even to explain such complex phenomena as cellular responses to synthetic surfaces in culture media or simulated medical device service environments.¹⁵ However, in many complex biological scenarios, other factors become important as well.¹⁶ Unfortunately, the surfactant adsorption processes are challenging to study experimentally, in particular, because the adsorbing layers are typically below a few nanometers in thickness, often comprising a single molecular monolayer.^{17–20}

An important effect of adsorbed molecules is that they reduce the surface tension of the interface to which they adsorb,^{21,22} which is why surfactants are often used to enhance the wetting ability of aqueous solutions²³ and to suppress hydrophobic cavitation.^{24,25} Surface-active molecules can dramatically alter the substrate wettability, and therewith leading to phenomena such as superspreading²⁶ or autophobing (spontaneous retraction of a drop after initial spreading).^{27,28} Determining the relationship between the surface tension and the structures of surfactant additives at different temperatures, pressures, salinities, and pH regimes is critical for the design in many industry sectors, ranging from consumer chemicals to oil and gas extraction.^{29,30} In recent years, we witnessed an enormous interest in surfactant-containing droplets, where the surfactant’s adsorption to the solid–water and air–water interface can render wetting in a nontrivial way.^{31–39}

Among the vast number of additives, alcohols hold a special place, being by far the most frequently used.⁴⁰ Short-chained alcohols are the simplest molecules that contain both hydrophobic and hydrophilic groups and are therefore excellent model systems in studies of interfaces.^{41–45} Alcohols are the most common cosurfactants added to surfactant and oil systems, for instance, in microemulsions. Alcohol adsorption is also relevant to distillation,⁴⁶ biofuels,⁴⁷ biomass transformation,⁴⁸ pharmacological processes (binding to membranes and proteins),^{49–51} and in aerosol science.^{52,53}

In this work, we employ molecular dynamics (MD) simulations to study how short-chained alcohols (*i.e.*, methanol, 1-propanol, and 1-pentanol) adsorb to two kinds of interfaces: water–vapor and solid–water. For the latter we used surfaces with various levels of hydrophilicity, characterized by dif-

ferent wetting coefficients (the cosine of the water contact angle).^{54,55} The three linear alcohols are very well soluble in water,⁵⁶ which enables studying the effect of chain length directly. Since they adsorb to both interfaces and lower their surface tension, we will refer to them also as surfactants⁵⁷ in this study. We compute the adsorption of alcohols onto the interfaces and analyze their dependence on the chain length and the surface contact angle, θ , expressed in terms of the wetting coefficient, $\cos \theta$. We invoke a continuum-level approach to rationalize the observed relationship between the adsorption and the wetting coefficient. Furthermore, using the Gibbs adsorption-isotherm formalism, we relate the surfactant adsorption to the decrease in the surface tensions. This enables us to analyze the variation of droplet contact angles in the dependence of the surfactant concentration.

2. METHODS

2.1. Atomistic models. We used the simple point charge/extended (SPC/E) model for water⁵⁸ combined with the GROMOS force field⁵⁹ for simulating alcohols and the solid surface. The all-atom structures and topology files for alcohols were obtained from the ATB repository.⁶⁰

To simulate the adsorption at the water–vapor interface, we set up an NVT (fixed number of particles, volume, and temperature) simulation with box dimensions of 5 nm \times 5 nm \times 10 nm with a water slab (containing various number of alcohol molecules) of thickness 5 nm in the middle (see Fig. 1b). Periodic boundary conditions were applied in all three directions. The vapor layer (of thickness 5 nm) was large enough such that the water slab did not interfere with its periodic images along the z direction.

For the planar solid surface, we adopted an atomistic model introduced before,^{61–63} which mimics a self-assembled monolayer. The surface was composed of restrained, hexagonally packed aliphatic chains terminated by hydroxyl (OH) head groups with the area density of 4.3 nm⁻². For the aliphatic chains, the united-atom representation was used. To generate different hydrophilicities of the surface, we rescaled the original partial charges in the OH groups by the factors 0, 0.4, 0.6, 0.7, and 0.8, which results in the water contact angles of the surface of $\theta = 135^\circ$, 120° , 97° , 76° , and 45° , respectively, as determined previously.⁶³ A 5-nm-thick water slab with added surfactant molecules was placed in contact with the surface. The simulation box (of lateral dimensions 5.2 nm \times 4.5 nm and height 10 nm) was replicated in all three directions *via* periodic boundary conditions (see Fig. 1c).

2.2. Simulations and data analysis details. The MD simulations were performed with the GROMACS 2019 simulation package.⁶⁴ The temperature was maintained at 300 K using the velocity-rescaling thermostat⁶⁵ with a time constant of 0.1 ps. In NPT (fixed number of particles, pressure, and temperature) simulations (used for the Kirkwood–Buff integrals), the pressure was controlled with the Parrinello–Rahman barostat^{66,67} of time constant 1.0 ps. Electrostatics was treated using particle-mesh-Ewald methods^{68,69} with a

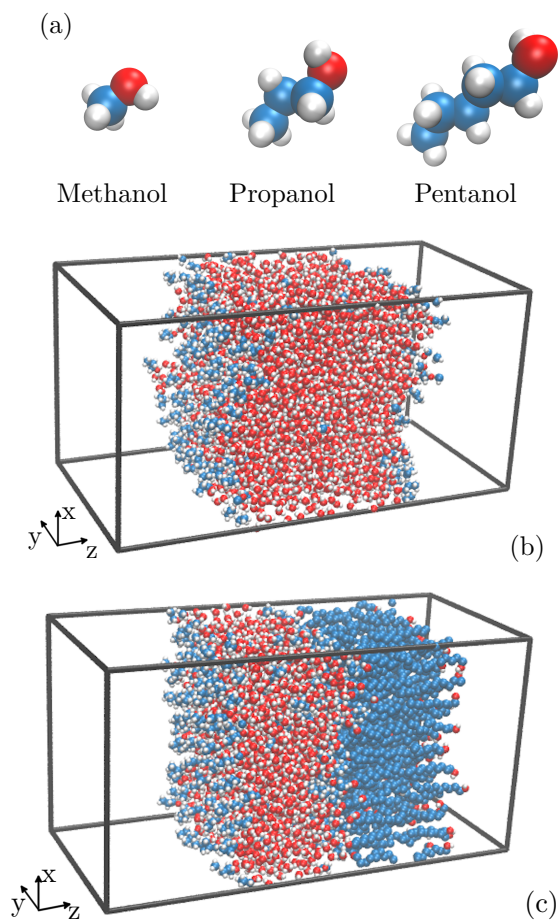


Figure 1: Simulation models. (a) Surfactant molecules in this work: methanol, 1-propanol, and 1-pentanol. (b) Simulation box of a water slab containing surfactant molecules, used to study the water–vapor adsorption. (c) Simulation box of a water slab in contact with the planar surface.

real-space cutoff of 0.9 nm. The LJ potentials were cut off at 0.9 nm in order to be compatible with the previous studies.^{61–63} The simulation times spanned up to 300 ns (3 independent realizations of 100 ns) for the water–vapor systems and 100 ns for the surface systems.

When performing fits of our data with a given function we use an orthogonal distance regression algorithm,⁷⁰ which allows to include the uncertainty of the data in both the x and y -coordinate. This is necessary since, for some set of data, the relative uncertainty is much larger for the x -coordinate.

3. RESULTS AND DISCUSSIONS

3.1. Adsorption at the water–vapor interface. We start by examining the adsorption behavior at the water–vapor interface (a proxy for the air–water interface), which is one of the most studied interfaces.^{45,46,56} Figure 2 shows normalized density profiles of water [$c_w(z)/c_{w0}$; dashed lines] with various concentrations of surfactant [$c(z)/c_0$; solid lines] in the proximity of the liquid–vapor interface. The pronounced den-

sity peaks of surfactants at the interface indicate preferential adsorption.

The adsorption is commonly quantified as the surface excess number density Γ of the surfactant across the effective water–vapor boundary,

$$\Gamma = \int_{-\infty}^{z_d} dz c(z) + \int_{z_d}^{\infty} dz [c(z) - c_0], \quad (1)$$

where c_0 is the bulk surfactant concentration and z_d denotes the position of the Gibbs dividing surface of water (*i.e.*, the position at which the excess water adsorption vanishes).

In Fig. 3, we plot evaluated adsorptions Γ as a function of the bulk concentration c_0 for all three alcohol surfactants. Generally, at first a linear trend for low concentrations starts leveling off at higher concentrations, which can be well described by the Langmuir adsorption isotherm^{21,71–73}

$$\Gamma = \Gamma_{\infty} \frac{k_c c_0}{1 + k_c c_0}, \quad (2)$$

shown in Fig. 3 and where k_c and Γ_{∞} are fitting parameters. For low concentrations, eq (2) reduces to Henry’s law,

$$\Gamma = K c_0 \quad (3)$$

where $K = k_c \Gamma_{\infty}$ is the adsorption coefficient. We denote the latter as K_v when representing the adsorption coefficient to the water–vapor interface and K_s to the solid–water interface. Henry’s law is also shown in Fig. 3 for comparison, with the adsorption coefficient K_v as obtained from the fit of the Langmuir isotherm. The adsorption coefficient K_v , as well as k_c , grows rapidly with molecular size: starting from $K_v = 0.8$ nm for methanol, 21 nm for propanol, and 410 nm for pentanol. Experimental values, obtained from literature^{21,71,74} (and references therein), for propanol and pentanol are $K_v = 32$ nm and 270 nm, respectively, which is in good agreement with the MD result given the high sensitivity on size, as we will see later on.

In contrast, the resulting saturation values of Γ_{∞} are comparable for the three alcohol species (6.52 nm⁻² for methanol, 5.06 nm⁻² for propanol and 4.80 nm⁻² for pentanol) because the adsorbed molecules occupy similar areas. Experimental data give $\Gamma_{\infty} \simeq 3.5$ nm⁻² for propanol and pentanol^{21,71} (and references therein), which also compares reasonably well to our MD results. Note that the accuracy of Γ_{∞} is not very high because of very few data points at high concentrations. A notable effect of surfactant adsorption at the water–vapor interface is that it reduces the surface tension, γ . The reduction is calculated by the Gibbs adsorption equation, $d\gamma = -\Gamma d\mu$, where μ is the surfactant chemical potential. Both Γ and μ depend on the concentration of surfactants, c_0 . Whereas for $\Gamma(c_0)$, we assume the Langmuir isotherm (eq 2), for the chemical potential we invoke the Kirkwood–Buff (KB) relation,^{75–77}

$$\left(\frac{\partial c_0}{\partial \mu} \right)_{T,P} = \frac{c_0 + c_0^2 (\mathcal{G}_{mm} - \mathcal{G}_{wm})}{k_B T} \quad (4)$$

where k_B is the Boltzmann constant, T the temperature, and \mathcal{G}_{mm} and \mathcal{G}_{wm} are the molecule–molecule and water–molecule KB integrals, defined as

$$\mathcal{G}_{ij} = \int_0^{\infty} [g_{ij}(r) - 1] 4\pi r^2 dr \quad (5)$$

where $g_{ij}(r)$ is the radial distribution function between species i and j in bulk. Evaluated $g_{ij}(r)$ in bulk solutions and calculated KB integrals \mathcal{G}_{mm} and \mathcal{G}_{wm} are shown in sec. S-1 of the Supplementary Information (SI). Both KB integrals are roughly constant for low concentrations. Therefore, we can combine eqs 2 and 4 with the Gibbs adsorption equation. After integration, we obtain the relation between the surface tension reduction $\Delta\gamma$ and the adsorption Γ

$$\Delta\gamma = \frac{k_B T \Gamma_{\infty}}{\xi} \ln \left(1 - \xi \frac{\Gamma}{\Gamma_{\infty}} \right) \quad (6)$$

with the correction factor

$$\xi = 1 - \frac{\Gamma_{\infty} (\mathcal{G}_{mm} - \mathcal{G}_{wm})}{K_v} \quad (7)$$

The correction factor ξ amounts to ~ 0.650 for methanol, ~ 0.950 for propanol, and ~ 0.998 for pentanol. Let us briefly discuss the dependence of ξ on surfactant size. Denoting the linear size of the molecule as l , Γ_{∞} roughly scales as $\sim l^{-2}$ (*i.e.*, corresponding to the tightly packed monolayer of surfactants) and for non-aggregating molecules $\mathcal{G}_{mm} - \mathcal{G}_{wm} \sim l^3$ (*i.e.*, corresponding to the volume of the surfactant). The product of the two scales with the size of the molecule, $\Gamma_{\infty} (\mathcal{G}_{mm} - \mathcal{G}_{wm}) \sim l$. As we will see, the adsorption coefficient K_v increases exponentially with molecular size, therefore the correction ξ is important for small molecules, whereas for larger molecules, it tends to unity, $\xi \rightarrow 1$; consistent with the simulation results.

In the limit of low adsorption (*i.e.*, $\Gamma \ll \Gamma_{\infty}$, relevant at low concentrations), eq 6 simplifies to a linear form

$$\Delta\gamma \simeq -k_B T \Gamma \quad (8)$$

which follows directly from Henry’s law⁷⁸ and by assuming ideal behavior of the chemical potential. The second-order term in the above expansion is $-(k_B T \xi / 2 \Gamma_{\infty}) \Gamma^2$, from which it follows that eq 8 is expected to be valid for $\Gamma \ll \xi^{-1} \Gamma_{\infty}$ (*i.e.*, when the second-order term is much smaller than the first term). Figure 4 shows the relation between the surface-tension reduction $\Delta\gamma$ and the surfactant adsorption Γ as obtained from the simulations (calculated from the diagonal pressure-tensor components⁷⁹) and theory (eqs 6 and 8). For small adsorption, the simple linear relation given by eq 8 (dotted line) matches very well the MD data. For higher adsorptions, the surface tension progressively sinks with adsorption, which is considerably well captured by the nonlinear relation (eq 6). However, some deviations are observed for intermediate values of Γ for propanol and pentanol. Clearly, the underlying theoretical assumptions have limitation, one of which is the use of the Langmuir isotherm, especially for

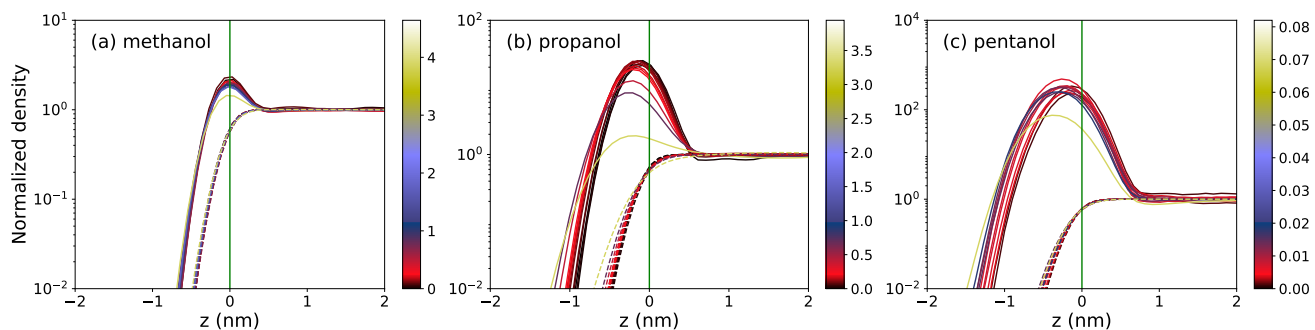


Figure 2: Normalized water (dashed lines) and surfactant (solid lines) density profiles (in logarithmic plot) at the water–vapor interface for different concentrations of (a) methanol, (b) propanol, and (c) pentanol. Different colors correspond to different bulk concentrations c_0 of the surfactant shown by the color bar on the right in the unit of nm^{-3} . The green vertical lines indicate the Gibbs dividing surface of the water phase.

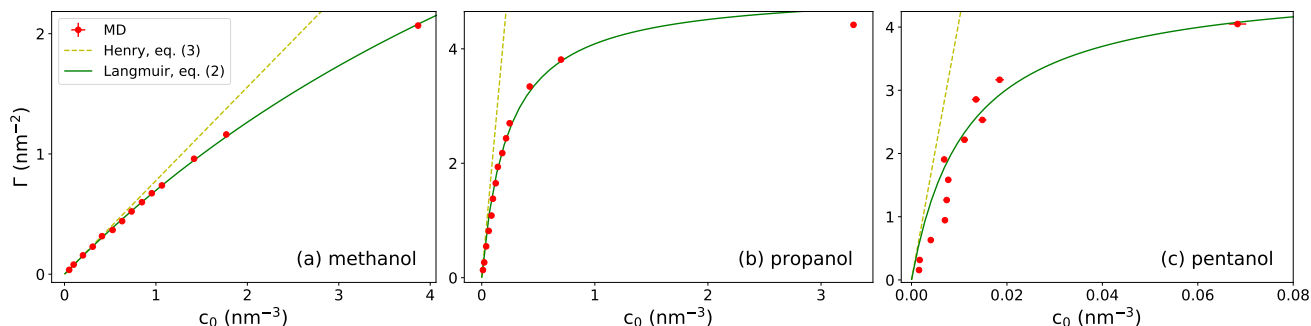


Figure 3: Adsorption Γ at the water–vapor interface as a function of the bulk concentration of (a) methanol, (b) propanol, and (c) pentanol. The MD data (red symbols) are fitted with the Langmuir isotherm, eq 2 (green line). Yellow dashed lines correspond to Henry’s law (eq 3), for which the coefficient K_V is obtained from the Langmuir fit ($K_V = k_c \Gamma_\infty$).

fitting the pentanol data (Fig. 2c). The agreement could probably be improved by considering more complex isotherms with more fitting parameters (*e.g.*, Frumkin isotherm),^{21,24,72} but this is beyond the scope of this study, which focuses rather on low-adsorption regimes.

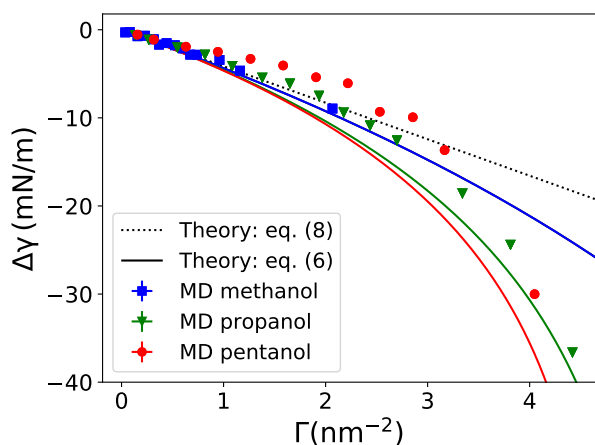


Figure 4: Reduction of the water–vapor surface tension *versus* adsorption as obtained from MD simulations (symbols) and theoretical predictions: eq 6 (solid lines) and its linear expansion eq 8 (dotted line).

3.2. Adsorption onto solid surfaces. We now turn our attention to solid surfaces and investigate how changing the polarity, manifesting in different contact angles ($\theta \simeq 45^\circ - 135^\circ$) affects the adsorption of the three surfactants. More details are provided in the Methods section and in refs. 61–63. We first take a look at some details of adsorption. Figure 5a is a snapshot of a pentanol molecule adsorbed on the hydrophobic surface with $\theta = 135^\circ$. The molecule partially penetrates into the surface interior by locally deforming the neighboring surface molecules. From the density profiles of this scenario, shown in Fig. 5b, we estimate that the molecule penetrates into the surface’s interior roughly by a half of its size. Similar behavior is also found for the other two alcohols and other surface polarities; see Fig. S-3 in the SI.

Following the same procedure as for the water–vapor adsorption, we evaluate the adsorption–concentration relations, a few representative examples of which are shown in Fig. 6 for a mildly hydrophobic surface with $\theta = 97^\circ$ (the rest can be found in sec. S-2 of the SI). The overall qualitative behavior is the same as at the water–vapor interface and it can be likewise well described by the Langmuir isotherm (shown by solid lines in Fig. 6). The values of Γ_∞ are shown in Fig. S-7 in the SI.

In Fig. 7a, we plot the adsorption coefficients onto the surface, K_s , against the surface wetting coefficient, $\cos \theta$. The outcomes clearly show that the hydrophobic surfaces have

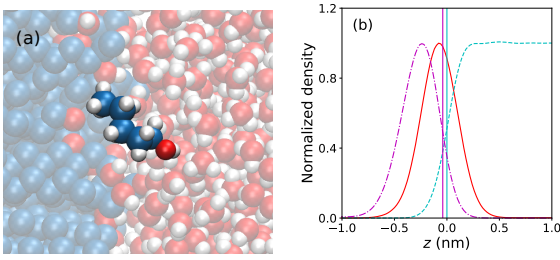


Figure 5: (a) Snapshot of an adsorbed pentanol molecule on the nonpolar surface with $\theta = 135^\circ$. (b) Corresponding rescaled density profiles of pentanol (red solid line) with bulk concentration of $c_0 = 0.001 \text{ nm}^{-3}$, the surface OH groups (magenta dash-dotted line), and water (cyan dashed line). Effective phase boundaries are depicted by the Gibbs dividing surface for water (cyan) and the position at half height on the water side of the OH group (magenta).

a much higher propensity to molecular adsorption than hydrophilic surfaces, which is consistent with the overall adsorption correlation with the contact angle found in various contexts.^{9,14,80,81} Moreover, the results even suggests an approximate quantitative relation of the form $\log K_s \sim \cos \theta$, which we will rationalize in the following.

Since the adsorption increases with chain length, which is hydrophobic, the driving mechanism should be the hydrophobic effect.²⁰ In order to at least qualitatively explain the observed relation, we resort to a continuum description of adsorption, schematically depicted in Fig. 8a: a surfactant molecule (m) adsorbs from bulk water (w) to the soft surface (s) by partially penetrating inside. The free energy of this adsorption scenario is composed of two contributions. Upon adsorption, the surfactant molecule forms direct contact with the surface of area A_c . In doing so, the water molecules in this area of the surfactant molecule had to be removed. The corresponding free energy change is $-A_c \gamma_{mw}$, where γ_{mw} is the molecule–water surface tension. The other contribution comes from new contacts between the molecule and the surface. However, even though the overall contact area with the surface is A_c , the surface area with the OH head groups is equal to the cross-sectional area of the molecule A_c^* . The surplus $A_c - A_c^*$ comes from the hydrocarbon groups hitherto buried inside the surface that are now exposed to the surfactant (see Fig. 8b for illustration). Because the surfactant molecule is predominantly also hydrocarbon (an alkyl chain), the surface surplus does not contribute to the excess surface free energy. The free energy contribution due to the new contacts is therefore $A_c^*(\gamma_{sm} - \gamma_{sw})$, where γ_{sm} and γ_{sw} are solid–molecule and solid–water surface tensions, respectively. Summing up both contributions gives the adsorption free energy of the surfactant molecule in the continuum, macroscopic picture as

$$\Delta G_s = A_c^*(\gamma_{sm} - \gamma_{sw}) - A_c \gamma_{mw} \quad (9)$$

Fig. 8b outlines the essential molecular rearrangements during the adsorption. The effective cross-sectional area A_c^* , which is the area of the removed water molecules from the surface, is best described by the cross section of the bare

molecule. If we approximate the molecule by a sphere (*i.e.*, $A_m = 4\pi R_m^2$ and $A_c^* = \pi R_m^2$, where R_m is its radius), then the cross-sectional area is $A_c^* = \frac{1}{4} A_m$. In the other extreme limit, in which the molecule is considered as an infinitely long cylinder (*i.e.*, $A_m = 2\pi R_m L$ and $A_c^* = 2R_m L$, where R_m is the radius and L the length of the cylinder), the relation becomes $A_c^* = \pi^{-1} A_m$. In realistic cases of finite rod-like molecules (such as alcohols in our case), the ratio A_c^*/A_m lies somewhere between the two extremes of $1/4 = 0.25$ and $1/\pi \approx 0.32$, which is a rather narrow interval. Since the continuum approach for describing molecular details is very approximate, we will assume the spherical approximation in the forthcoming analysis.

Before proceeding with eq 9, we have to be aware that applying macroscopic concepts of interfacial surface at the molecular level is in general a delicate move. Nonetheless, some problems can be, at least qualitatively, formally resolved by identifying effective molecular surface areas and curvature (*i.e.*, Tolman) corrections to surface tensions.^{82,83} Such an analysis reaches, however, far beyond the scope of this study. Therefore, we will use the above continuum equation only to extract the dependence of adsorption on the contact angle. The latter is related to removal of water from the flat area of the solid, whose surface is flat (requiring no curvature corrections) and whose surface tension is macroscopically well defined.

The solid–water surface tension γ_{sw} is the only quantity in eq 9 that depends on the contact angle. The dependence is provided by the Young equation of a water droplet on the surface,

$$\gamma_{sw} = \gamma_{sv} - \gamma \cos \theta \quad (10)$$

where γ_{sv} is the solid–vapor surface tension. Equation 9 now expresses as

$$\Delta G_s = \Delta G_s^{(0)} + \frac{1}{4} A_m \gamma \cos \theta \quad (11)$$

where the reference value $\Delta G_s^{(0)} = A_c^*(\gamma_{sm} - \gamma_{sv}) - A_c \gamma_{mw}$ is the adsorption free energy to the surface with a vanishing a wetting coefficient, $\cos \theta = 0$ (*i.e.*, for $\theta = 90^\circ$). The above equation nicely demonstrates the modulation of the adsorption free energy with the contact angle.

From a known ΔG_s , the adsorption coefficient to the surface can be estimated as

$$K_s = b_s e^{-\beta \Delta G_s} \quad (12)$$

where $\beta = 1/k_B T$ and b_s is a fitting parameter. Using eq 11, the dependence of the adsorption coefficient on $\cos \theta$ follows as

$$K_s = K_s^{(0)} \exp\left(-\frac{1}{4} \beta A_m \gamma \cos \theta\right) \quad (13)$$

where the reference $K_s^{(0)} = b_s \exp(-\beta \Delta G_s^{(0)})$ is the adsorption coefficient for the surface with vanishing wetting coefficient. As seen in Fig. 7a, the agreement between the MD data and eq 13 (with $K_s^{(0)}$ as a fitting parameter to the middle data points) is reasonably good, particularly in the hydropho-

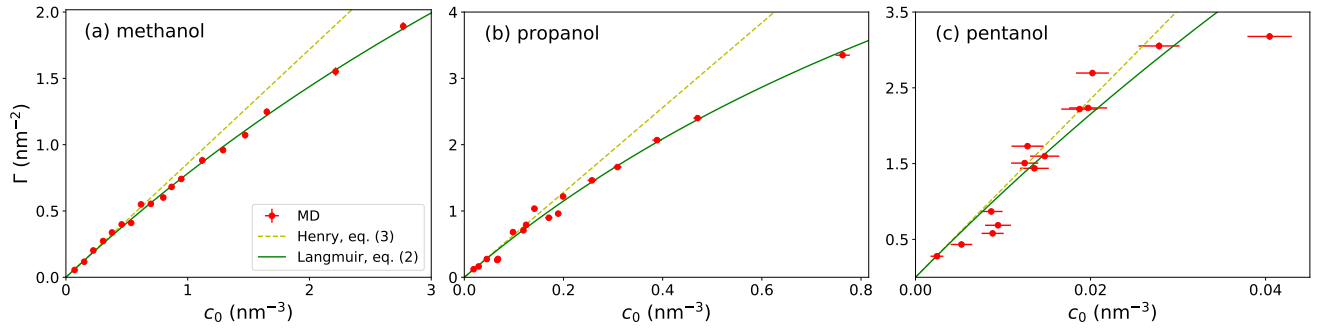


Figure 6: Adsorption onto the surface with a wetting contact angle of $\theta = 97^\circ$ as a function of the bulk concentration of (a) methanol, (b) propanol, and (c) pentanol. MD values are shown by red circles, whereas solid green lines show the fits of the Langmuir isotherm. Yellow dashed lines correspond to Henry's law (eq 3), for which the coefficient K_v is taken from the Langmuir fit.

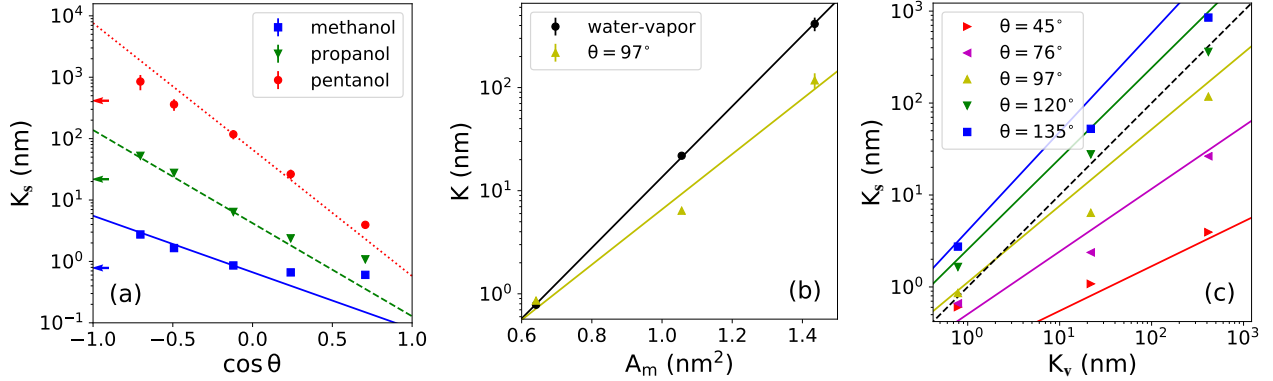


Figure 7: Adsorption coefficients. (a) Adsorption coefficient *versus* wetting coefficient for all three alcohols. The lines are predictions of eq 13, whereby the coefficient $K_s^{(0)}$ (controlling the offset) was used as a fitting parameter to the middle data points, with the wetting coefficient closest to zero ($\cos \theta = -0.12$). The arrows indicate the adsorption coefficients to the water-vapor interface, K_v . (b) Adsorption coefficient $K_s^{(0)}$ for vanishing wetting coefficient *versus* molecular surface area A_m . A comparison with the the water-vapor interface K_v is also shown. The solid lines are fitted exponential functions (eqs 14 and 15), which give $\tilde{\gamma}_s \simeq 25.6$ mN/m and $\tilde{\gamma}_v \simeq 32.7$ mN/m. (c) Correlation between adsorption coefficient to the solid surface (K_s) and to the water-vapor interface (K_v). The symbols are MD results, solid lines are predictions of eq 16. The dashed diagonal line denotes the symmetric case $K_s = K_v$.

bic regime ($\cos \theta < 0$). For hydrophilic cases ($\cos \theta > 0$), agreement becomes worse, especially for smaller molecules such as methanol, which exhibit weak adsorption. One reason for the poorer agreement is that in weakly-adsorbing cases (*i.e.*, small K_s), the molecule penetrates less into the surface (see Fig. S-3 in the SI), thus A_m^* is smaller than $A_m/4$. The next relevant question is, how does the reference adsorption coefficient $K_s^{(0)}$ depend on the molecular surface area. In Fig. 7b, we plot the relation between $K_s^{(0)}$ and the molecular surface area A_m . The result can be easily understood using eq 9, which suggests that the adsorption free energy is proportional to the molecular surface area, $\Delta G_s^{(0)} = -\tilde{\gamma}_s A_m$, where the proportionality coefficient $\tilde{\gamma}_s$ can be considered as an effective molecular surface tension for adsorption.^{82,83} For the reference adsorption coefficient we can thus write

$$K_s^{(0)} = b_s e^{\beta \tilde{\gamma}_s A_m} \quad (14)$$

and likewise, for the adsorption coefficient at the water-vapor interface

$$K_v = b_v e^{\beta \tilde{\gamma}_v A_m} \quad (15)$$

The above two equations fit the MD data points in Fig. 7b very well, with b_i and $\tilde{\gamma}_i$ ($i = v, s$) used as fitting parameters. It is insightful to look at the correlation between the adsorption coefficients to both interfaces K_s and K_v , as plotted in Fig. 7c. The two coefficients are very well correlated for a given surface contact angle, implying that the better a molecule adsorbs onto the water-vapor interface, the better it adsorbs onto the solid surface. This correlation stems primarily from the linear dependence of adsorption energies on molecular surface area. Using eqs 13–15 and eliminating A_m , we come up with the following analytic relation

$$\ln \frac{K_s}{b_s} = \frac{\tilde{\gamma}_s - \frac{1}{4}\gamma \cos \theta}{\tilde{\gamma}_v} \ln \frac{K_v}{b_v} \quad (16)$$

which demonstrates that, indeed, the logarithms of the two adsorption coefficients are linearly related, with a prefactor that linearly decreases with $\cos \theta$. Using the fitted coefficients from Fig. 7b, we plot the predictions of eq 16 in Fig. 7c as solid lines. Even though the agreement is not perfect, the slope is nicely captured by the prefactor of eq 16, at least for the larger two alcohols.

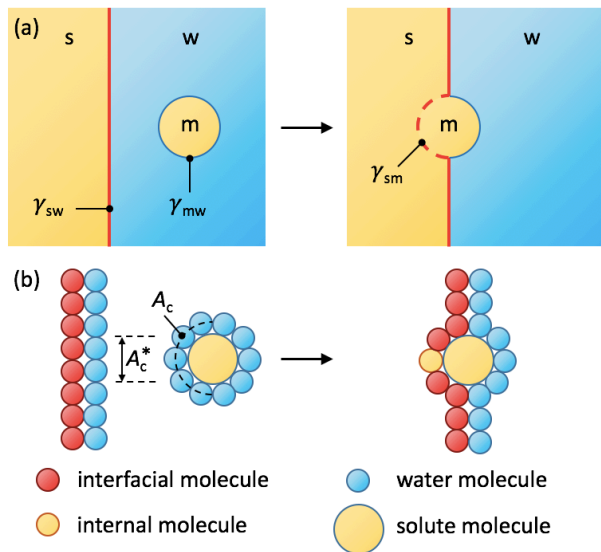


Figure 8: Schematic depiction of molecular adsorption to a soft surface. (a) Continuum picture: Adsorption is governed by surface tensions between the molecule (m), water (w), and the surface (s). (b) Molecular picture: The relevant areas are the bare cross sectional surface area of the molecule (A_c^*) and the surface-accessible contact surface area (A_c).

From the correlation plot, we conclude that the adsorption to the water–vapor interface is always stronger than to the polar solid surfaces with contact angles below $\theta \approx 97^\circ$ — the data lie below the diagonal symmetry line. Moreover, the ratio K_s/K_v becomes progressively smaller with an increasing K_v (*i.e.*, molecular size). In contrast, the hydrophobic surfaces with contact angles above $\theta \approx 120^\circ$ outdo the water–vapor interface in adsorption, at least for not too large and too strongly adsorbing molecules. Qualitatively same trends were experimentally observed on hydrophobic and mildly hydrophilic surfaces.^{44,84}

Surfactant effect on the wetting contact angle. In the end, we take a look at a scenario where the adsorption to the water–vapor and a solid surface compete with each other — a sessile water droplet containing surfactants. A neat water droplet deposited on a solid surface forms the contact angle θ with the surface, given by the Young equation (eq 10). When surfactant is introduced into the droplet, it adsorbs to both interfaces, solid–water and water–vapor, thereby reducing their surface tensions, which become dependent on the surfactant concentration (*i.e.*, $\gamma_{sw}(c_0)$ and $\gamma(c_0)$). In principle, less soluble surfactants can also adsorb at the solid–vapor interface,³⁹ which does, however, not occur in our case (see sec. S-3 of the SI). Consequently, the solid–vapor surface tension, γ_{sv} , remains unaffected. The Young equation of the surfactant-laden droplet then reads^{27,37}

$$\cos(\theta + \Delta\theta) = \frac{\gamma_{sv} - \gamma_{sw}(c_0)}{\gamma(c_0)} \quad (17)$$

where θ is the contact angle of the neat (surfactant-free) water droplet and $\Delta\theta$ is the change of the contact angle due to the surfactant. For small changes in contact angle ($\Delta\theta \ll 1$), the above equation simplifies to

$$\Delta\theta \simeq \frac{\Delta\gamma_{sw} + \Delta\gamma \cos \theta}{\gamma \sin \theta} \quad (18)$$

In the linear adsorption regime, in which Henry’s law and eq 8 apply, the expression further simplifies to

$$\Delta\theta \simeq -k_B T \frac{K_s + K_v \cos \theta}{\gamma \sin \theta} c_0 \quad (19)$$

which is a modification of the Lucassen–Reynders equation.⁸⁵

In Fig. 9, we show the predictions of the contact angle change for all three alcohols and for different surface hydrophilicities, based on eq 17 (solid lines) and its linearized version, eq 19 (dashed lines). In eq 17, we used eq 6 for calculating the surface tension reduction of both interfaces. We see that in all cases, the contact angle θ monotonically decreases with the bulk surfactant concentration in the droplet. That is, adding surfactant enhances wetting. The $\Delta\theta$ vs. c_0 relation is altogether linear at first, as predicted by eq 19, and becomes nonlinear at higher concentrations: Sublinear on hydrophobic surfaces and superlinear on hydrophilic ones.

Interestingly, the change in contact angle drastically and non-monotonically depends on the surface hydrophilicity, given by $\cos \theta$, as even better demonstrated in Fig. 10. The non-monotonicity results from the competition between the adsorptions onto the water–vapor and solid–water interfaces of the droplet and is encoded in the numerator of eq 19, reading $K_s(\theta) + K_v \cos \theta$. On considerably hydrophilic surfaces (small θ), the adsorption of surfactants onto the surface is negligible (*i.e.*, $K_s \ll K_v$) and thus the surfactant effect is dominated by the adsorption onto the water–vapor interface, dictated by the term $K_v \cos \theta$ in eq 19. In this regime, the change in the contact angle scales as $\Delta\theta \propto -\cot \theta$. The effect of surfactant becomes extremely large for small contact angles, and it even diverges as the surface approaches the complete wetting regime ($\theta \rightarrow 0^\circ$). This means that already low concentrations of surfactant in a low-contact angle droplet can easily push the droplet into the complete wetting regime. This observation also suggests that measurements of small contact angles are particularly challenging because of potential contamination of aqueous systems with surface-active molecules.^{21,86,87}

With increasing hydrophobicity (increasing θ), the surface adsorption coefficient K_s rapidly increases (see Fig. 7b and eq 13) and eventually exceeds K_v . Thus, $|\Delta\theta|$ starts dramatically rising with the surface hydrophobicity. Our analysis also shows that surfaces with contact angles around $\theta = 90^\circ$ are the least sensitive to wetting alterations due to surfactants as compared to hydrophilic or hydrophobic surfaces.

Markedly, the net effect of adding simple alcohols to water is always to decrease the contact angle of the droplet ($\Delta\theta < 0$), even though this is not strictly imposed by eq 19. Most ex-

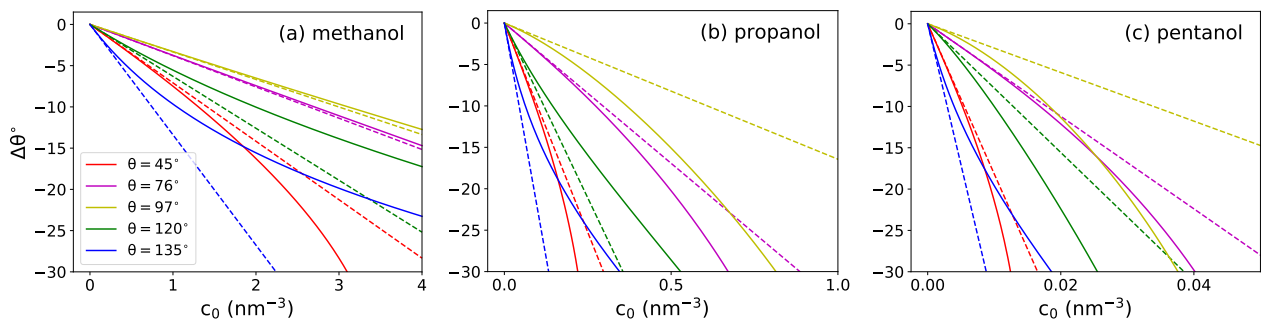


Figure 9: Change of the contact angle $\Delta\theta$ due to surfactant adsorption as a function of surfactant concentration for (a) methanol, propanol, and (c) pentanol on surfaces with different contact angles. Solid lines are predictions of eq (17) and dashed lines are low-concentration predictions given by eq (19).

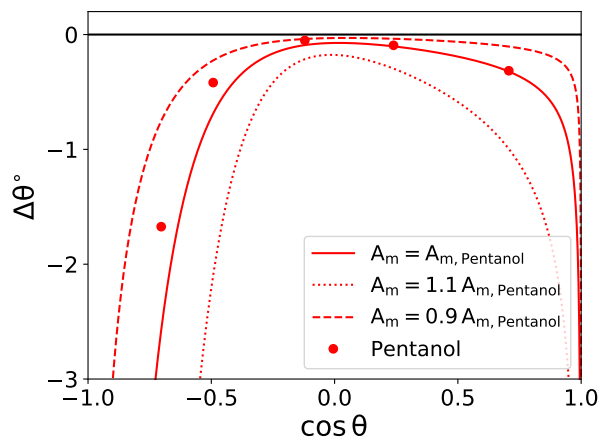


Figure 10: Change in the water contact angle as a function of wetting coefficient for $c_0 = 0.01 \text{ nm}^{-3}$ of added pentanol based on eq (19). The symbols are obtained by using K_v and $K_s^{(0)}$ from the simulations of pentanol. The lines are obtained using the predictions of eqs (13), (14), and (15) for K_v and K_s and three different values for the molecular surface area A_m .

perimental studies show that surfactants decrease the contact angle of aqueous solutions on hydrophobic surfaces.^{22,44,84} Theoretically, the effect could be positive ($\Delta\theta > 0$) for hydrophobic surfaces (for which $\cos\theta < 0$) if the adsorption onto the surface remains small, such that $K_s > -K_v \cos\theta$, which is, however, not the case in our systems.

4. CONCLUSIONS

We investigated the adsorption of short-chained alcohols (simple surfactants) onto two types of interfaces, the water-vapor and solid-water. The solid surface included various levels of polarity, which manifested in a broad span of water contact angles. We have analyzed how the adsorption depends on the surface contact angle. Adsorption properties calculated from MD simulations follow very well the Langmuir adsorption isotherm for most of the studied cases, except for some smaller deviations in the case of pentanol. We have found that the adsorption coefficient onto the solid surface

scales roughly exponentially with the molecular surface area and the surface wetting coefficient (eq 13). Based on the continuum-level description, this dependence arises from the free energy of removing water molecules from the contact area of the surface with the adsorbing surfactant molecule. In addition, we have shown a unique and practical correlation between the water-vapor and the water-solid adsorptions (Fig. 7c), which can also assist in estimating the solid-water adsorption based on the water-vapor adsorption.

The competition between the adsorption at the solid-water and water-vapor interface manifests by far the most directly in the contact angles of water droplets containing surfactants. Our theoretical analysis suggests that the short-chained alcohols in all our cases reduce the contact angle and, with that, enhance wetting. The wetting enhancement depends drastically and non-monotonically on the wetting coefficient. We have found high sensitivity of the contact angle on surfactant concentration on very hydrophilic surfaces, which can easily cross the complete wetting regime. A strong influence of surfactants is also observed for very hydrophobic surfaces, owing to strong surfactant adsorption to the surface. In contrast, mildly polar surfaces, with contact angles around 90° , are much less sensitive to wetting alterations.

The outcomes of this study are also relevant to further experimental efforts at the nanoscale, in which tuning the surfactant concentration is used to improve liquids' sticking or coverage on solids, such as in detergency, inkjet printing, or pesticide spraying. Surface-active pharmacological agents could be used to promote liquid spreading and treat or prevent bubble obstruction of blood flow.³¹ Surfactant uptake is also crucial for self-cleaning processes of hydrophobic surfaces by water drops.⁸⁸ Finally, making surface-active molecules charged brings about numerous electrochemical phenomena, which reflect, for instance, in zeta potential, nanobubble stability, and the Jones-Ray effect,⁸⁹ and which add a layer of complexity to wetting and would be interesting to investigate in future studies.

Acknowledgments. We acknowledge funding from the Slovenian Research Agency ARRS (Research Core Funding No. P1-0055 and Research Grant No. J1-1701).

References

- (1) Schmidt, D. L.; Brady, R. F.; Lam, K.; Schmidt, D. C.; Chaudhury, M. K. Contact Angle Hysteresis, Adhesion, and Marine Biofouling. *Langmuir* **2004**, *20*, 2830–2836, PMID: 15835160.
- (2) Li, S.; Du, L.; Wei, Z.; Wang, W. Aqueous-Phase Aerosols on the Air-Water Interface: Response of Fatty Acid Langmuir Monolayers to Atmospheric Inorganic Ions. *Sci. Total Environ.* **2017**, *580*, 1155–1161.
- (3) Salta, M.; Wharton, J. A.; Blache, Y.; Stokes, K. R.; Briand, J.-F. Marine Biofilms on Artificial Surfaces: Structure and Dynamics. *Environ. Microbiol.* **2013**, *15*, 2879–2893.
- (4) Encinas, N.; Yang, C.-Y.; Geyer, F.; Kaltbeitzel, A.; Baumli, P.; Reinholz, J.; Mailänder, V.; Butt, H.-J.; Vollmer, D. Submicrometer-Sized Roughness Suppresses Bacteria Adhesion. *ACS Appl. Mater. Interfaces* **2020**, *12*, 21192–21200, PMID: 32142252.
- (5) Singh, A. K.; Singh, P.; Mishra, S.; Shahi, V. K. Anti-Biofouling Organic-Inorganic Hybrid Membrane for Water Treatment. *J. Mater. Chem.* **2012**, *22*, 1834–1844.
- (6) Bera, A.; Kumar, T.; Ojha, K.; Mandal, A. Adsorption of Surfactants on Sand Surface in Enhanced Oil Recovery: Isotherms, Kinetics and Thermodynamic Studies. *Appl. Surf. Sci.* **2013**, *284*, 87 – 99.
- (7) Busca, G.; Berardinelli, S.; Resini, C.; Arrighi, L. Technologies for the Removal of Phenol from Fluid Streams: A Short Review of Recent Developments. *J. Hazard. Mater.* **2008**, *160*, 265 – 288.
- (8) Thierry, B.; Merhi, Y.; Bilodeau, L.; Trepanier, C.; Tabrizian, M. Nitinol Versus Stainless Steel Stents: Acute Thrombogenicity Study in an Ex Vivo Porcine Model. *Biomaterials* **2002**, *23*, 2997–3005.
- (9) Rosenhahn, A.; Schilp, S.; Kreuzer, H. J.; Grunze, M. The Role of “Inert” Surface Chemistry in mMrine Biofouling Prevention. *Phys. Chem. Chem. Phys.* **2010**, *12*, 4275–4286.
- (10) Tegenfeldt, J. O.; Prinz, C.; Cao, H.; Huang, R. L.; Austin, R. H.; Chou, S. Y.; Cox, E. C.; Sturm, J. C. Micro-and Nanofluidics for DNA Analysis. *Anal. Bioanal. Chem.* **2004**, *378*, 1678–1692.
- (11) Niedzwiecki, D. J.; Grazul, J.; Movileanu, L. Single-Molecule Observation of Protein Adsorption onto an Inorganic Surface. *J. Am. Chem. Soc.* **2010**, *132*, 10816–10822.
- (12) Prime, K. L.; Whitesides, G. M. Self-Assembled Organic Monolayers: Model Systems for Studying Adsorption of Proteins at Surfaces. *Science* **1991**, 1164–1167.
- (13) Sigal, G. B.; Mrksich, M.; Whitesides, G. M. Effect of Surface Wettability on the Adsorption of Proteins and Detergents. *J. Am. Chem. Soc.* **1998**, *120*, 3464–3473.
- (14) Vogler, E. A. Structure and Reactivity of Water at Biomaterial Surfaces. *Adv. Colloid Interface Sci.* **1998**, *74*, 69–117.
- (15) Bryk, P.; Korczeniewski, E.; Szymański, G. S.; Kowalczyk, P.; Terpiłowski, K.; Terzyk, A. P. What Is the Value of Water Contact Angle on Silicon? *Materials* **2020**, *13*.
- (16) Alexander, M. R.; Williams, P. Water Contact Angle is not a Good Predictor of Biological Responses to Materials. *Biointerphases* **2017**, *12*, 02C201.
- (17) Manne, S.; Gaub, H. E. Molecular Organization of Surfactants at Solid-Liquid Interfaces. *Science* **1995**, *270*, 1480–1482.
- (18) Paria, S.; Khilar, K. C. A Review on Experimental Studies of Surfactant Adsorption at the Hydrophilic Solid–Water Interface. *Adv. Colloid Interface Sci.* **2004**, *110*, 75 – 95.
- (19) Yoshimitsu, Z.; Nakajima, A.; Watanabe, T.; Hashimoto, K. Effects of Surface Structure on the Hydrophobicity and Sliding Behavior of Water Droplets. *Langmuir* **2002**, *18*, 5818–5822.
- (20) Sendner, C.; Horinek, D.; Bocquet, L.; Netz, R. R. Interfacial water at hydrophobic and hydrophilic surfaces: Slip, viscosity, and diffusion. *Langmuir* **2009**, *25*, 10768–10781.
- (21) Chang, C.-H.; Franses, E. I. Adsorption Dynamics of Surfactants at the Air/Water Interface: a Critical Review of Mathematical Models, Data, and Mechanisms. *Colloids Surf., A* **1995**, *100*, 1–45.
- (22) Starov, V. M.; Kosvintsev, S. R.; Velarde, M. G. Spreading of Surfactant Solutions over Hydrophobic Substrates. *J. Colloid Interface Sci.* **2000**, *227*, 185–190.
- (23) von Bahr, M.; Tiberg, F.; Zhmud, B. V. Spreading Dynamics of Surfactant Solutions. *Langmuir* **1999**, *15*, 7069–7075.
- (24) Diamant, H.; Andelman, D. Kinetics of Surfactant Adsorption at Fluid-Fluid Interfaces. *J. Phys. Chem.* **1996**, *100*, 13732–13742.
- (25) Meyer, E. E.; Rosenberg, K. J.; Israelachvili, J. Recent Progress in Understanding Hydrophobic Interactions. *Proc. Natl. Acad. Sci.* **2006**, *103*, 15739–15746.

- (26) Rafai, S.; Sarker, D.; Bergeron, V.; Meunier, J.; Bonn, D. Superspreading: Aqueous Surfactant Drops Spreading on Hydrophobic Surfaces. *Langmuir* **2002**, *18*, 10486–10488.
- (27) Bera, B.; Duits, M. H.; Stuart, M. C.; Van Den Ende, D.; Mugele, F. Surfactant Induced Autophobing. *Soft Matter* **2016**, *12*, 4562–4571.
- (28) Afsar-Siddiqui, A. B.; Luckham, P. F.; Matar, O. K. Dewetting Behavior of Aqueous Cationic Surfactant Solutions on Liquid Films. *Langmuir* **2004**, *20*, 7575–7582.
- (29) Sresht, V.; Lewandowski, E. P.; Blankschtein, D.; Jusufi, A. Combined Molecular Dynamics Simulation–Molecular-Thermodynamic Theory Framework for Predicting Surface Tensions. *Langmuir* **2017**, *33*, 8319–8329.
- (30) Halvey, A. K.; Macdonald, B.; Dhyani, A.; Tuteja, A. Design of Surfaces for Controlling Hard and Soft Fouling. *Philos. Trans. R. Soc., A* **2019**, *377*, 20180266.
- (31) Eckmann, D. M.; Cavanagh, D. P.; Branger, A. B. Wetting Characteristics of Aqueous Surfactant-Laden Drops. *J. Colloid Interface Sci.* **2001**, *242*, 386–394.
- (32) Bera, B.; Carrier, O.; Backus, E. H.; Bonn, M.; Shahidzadeh, N.; Bonn, D. Counteracting Interfacial Energetics for Wetting of Hydrophobic Surfaces in the Presence of Surfactants. *Langmuir* **2018**, *34*, 12344–12349.
- (33) Thiele, U.; Snoeijer, J. H.; Trinschek, S.; John, K. Equilibrium Contact Angle and Adsorption Layer Properties With Surfactants. *Langmuir* **2018**, *34*, 7210–7221.
- (34) Tadmor, R.; Baksi, A.; Gulec, S.; Jadhav, S.; N'guessan, H.; Sen, K.; Somasi, V.; Tadmor, M.; Wasnik, P.; Yadav, S. Drops that Change Their Mind: Spontaneous Reversal From Spreading to Retraction. *Langmuir* **2019**, *35*, 15734–15738.
- (35) Kwieceński, W.; Segers, T.; Van Der Werf, S.; Van Houselt, A.; Lohse, D.; Zandvliet, H. J.; Kooij, S. Evaporation of Dilute Sodium Dodecyl Sulfate Droplets on a Hydrophobic Substrate. *Langmuir* **2019**, *35*, 10453–10460.
- (36) Tadmor, R.; Multanen, V.; Stern, Y.; Yakir, Y. B. Drops Retracting While Forming a Rim. *J. Colloid Interface Sci.* **2021**, *581*, 496–503.
- (37) Sun, C.; Liu, M.; Xu, S.; Zhu, S.; Wu, J.; Bai, B. Ion-Induced Oil–Water Wettability Alteration of Rock Surfaces. Part I: Polar Interactions Between Oil and Solid. *Chem. Eng. Sci.* **2021**, *232*, 116366.
- (38) Henrich, F.; Fell, D.; Truszkowska, D.; Weirich, M.; Anyfantakis, M.; Nguyen, T.-H.; Wagner, M.; Auernhammer, G. K.; Butt, H.-J. Influence of Surfactants in Forced Dynamic Dewetting. *Soft Matter* **2016**, *12*, 7782–7791.
- (39) Bera, B.; Backus, E. H. G.; Carrier, O.; Bonn, M.; Shahidzadeh, N.; Bonn, D. Antisurfactant (Autophobic) Behavior of Superspreader Surfactant Solutions. *Langmuir* **2021**, *37*, 6243–6247.
- (40) Zana, R. Aqueous Surfactant-Alcohol Systems: A Review. *Adv. Colloid Interface Sci.* **1995**, *57*, 1 – 64.
- (41) Tarek, M.; Tobias, D. J.; Klein, M. L. Molecular Dynamics Investigation of the Surface/Bulk Equilibrium in an Ethanol-Water Solution. *J. Chem. Soc., Faraday Trans.* **1996**, *92*, 559–563.
- (42) Stewart, E.; Shields, R. L.; Taylor, R. S. Molecular Dynamics Simulations of the Liquid/Vapor Interface of Aqueous Ethanol Solutions as a Function of Concentration. *J. Phys. Chem. B* **2003**, *107*, 2333–2343.
- (43) Wilson, M. A.; Pohorille, A. Adsorption and Solvation of Ethanol at the Water Liquid-Vapor Interface: A Molecular Dynamics Study. *J. Phys. Chem. B* **1997**, *101*, 3130–3135, PMID: 11540504.
- (44) Szymczyk, K.; Zdziennicka, A.; Jańczuk, B.; Wójcik, W. The Wettability of Polytetrafluoroethylene and Polymethyl Methacrylate by Aqueous Solution of Two Cationic Surfactants Mixture. *J. Colloid Interface Sci.* **2006**, *293*, 172–180.
- (45) Hub, J. S.; Caleman, C.; van der Spoel, D. Organic Molecules on the Surface of Water Droplets—an Energetic Perspective. *Phys. Chem. Chem. Phys.* **2012**, *14*, 9537–9545.
- (46) Karlsson, B. C. G.; Friedman, R. Dilution of Whisky – the Molecular Perspective. *Sci. Rep.* **2017**, *7*, 6489.
- (47) Levario, T. J.; Dai, M.; Yuan, W.; Vogt, B. D.; Nielsen, D. R. Rapid Adsorption of Alcohol Biofuels by High Surface Area Mesoporous Carbons. *Microporous Mesoporous Mater.* **2012**, *148*, 107 – 114.
- (48) Corma, A.; Iborra, S.; Velty, A. Chemical Routes for the Transformation of Biomass into Chemicals. *Chem. Rev.* **2007**, *107*, 2411–2502, PMID: 17535020.
- (49) Seeman, P.; Roth, S.; Schneider, H. The Membrane Concentrations of Alcohol Anesthetics. *Biochim. Biophys. Acta, Biomembr.* **1971**, *225*, 171–184.
- (50) Bull, H. B.; Breese, K. Interaction of Alcohols With Proteins. *Biopolymers* **1978**, *17*, 2121–2131.

- (51) Peoples, R. W.; Chaoying, L.; Weight, F. F. Lipid vs Protein Theories of Alcohol Action in the Nervous System. *Annu. Rev. Pharmacol. Toxicol.* **1996**, *36*, 185–201, PMID: 8725387.
- (52) Tarbuck, T. L.; Richmond, G. L. Adsorption and Reaction of CO₂ and SO₂ at a Water Surface. *J. Am. Chem. Soc.* **2006**, *128*, 3256–3267, PMID: 16522107.
- (53) Szöri, M.; Roeselová, M.; Jedlovsky, P. Surface Hydrophilicity-Dependent Water Adsorption on Mixed Self-Assembled Monolayers of C7-CH₃ and C7-COOH Residues. A Grand Canonical Monte Carlo Simulation Study. *J. Phys. Chem. C* **2011**, *115*, 19165–19177.
- (54) Butt, H.-J.; Graf, K.; Kappl, M. *Physics and Chemistry of Interfaces*; Wiley, 2003.
- (55) Gillies, G.; Büscher, K.; Preuss, M.; Kappl, M.; Butt, H.-J.; Graf, K. Contact angles and wetting behaviour of single micron-sized particles. **2005**, *17*, S445–S464.
- (56) van der Spoel, D.; Wensink, E. J. W.; Hoffmann, A. C. Lifting a Wet Glass from a Table: A Microscopic Picture. *Langmuir* **2006**, *22*, 5666–5672, PMID: 16768492.
- (57) McNaught, A. D.; Wilkinson, A. *IUPAC. Compendium of Chemical Terminology, 2nd ed. (the “Gold Book”)*; Blackwell Scientific Publications, Oxford, 1997.
- (58) Berendsen, H. J. C.; Grigera, J. R.; Straatsma, T. P. The Missing Term in Effective Pair Potentials. *J. Phys. Chem.* **1987**, *91*, 6269–6271.
- (59) Oostenbrink, C.; Villa, A.; Mark, A. E.; van Gunsteren, W. F. A Biomolecular Force Field Based on the Free Enthalpy of Hydration and Solvation: The GROMOS Force-Field Parameter Sets 53A5 and 53A6. *J. Comput. Chem.* **2004**, *25*, 1656–1676.
- (60) Malde, A. K.; Zuo, L.; Breeze, M.; Stroet, M.; Poger, D.; Nair, P. C.; Oostenbrink, C.; Mark, A. E. An Automated Force Field Topology Builder (ATB) and Repository: Version 1.0. *J. Chem. Theory Comput.* **2011**, *7*, 4026–4037.
- (61) Kanduč, M.; Schneck, E.; Netz, R. R. Attraction Between Hydrated Hydrophilic Surfaces. *Chem. Phys. Lett.* **2014**, *610-611*, 375 – 380.
- (62) Kanduč, M.; Schlaich, A.; Schneck, E.; Netz, R. R. Water-Mediated Interactions between Hydrophilic and Hydrophobic Surfaces. *Langmuir* **2016**, *32*, 8767–8782, PMID: 27487420.
- (63) Kanduč, M. Going Beyond the Standard Line Tension: Size-Dependent Contact Angles of Water Nanodroplets. *J. Chem. Phys.* **2017**, *147*, 174701.
- (64) van der Spoel, D.; Lindahl, E.; Hess, B.; Groenhof, G.; Mark, A. E.; Berendsen, H. J. C. GROMACS: Fast, Flexible, and Free. *J. Comput. Chem.* **2005**, *26*, 1701–1718.
- (65) Bussi, G.; Donadio, D.; Parrinello, M. Canonical Sampling Through Velocity Rescaling. *J. Chem. Phys.* **2007**, *126*, 014101.
- (66) Parrinello, M.; Rahman, A. Polymorphic Transitions in Single Crystals: A New Molecular Dynamics Method. *J. Appl. Phys.* **1981**, *52*, 7182–7190.
- (67) Nosé, S.; Klein, M. Constant Pressure Molecular Dynamics for Molecular Systems. *Mol. Phys.* **1983**, *50*, 1055–1076.
- (68) Darden, T.; York, D.; Pedersen, L. Particle Mesh Ewald: An N log(N) Method for Ewald Sums in Large Systems. *J. Chem. Phys.* **1993**, *98*, 10089–10092.
- (69) Essmann, U.; Perera, L.; Berkowitz, M. L.; Darden, T.; Lee, H.; Pedersen, L. G. A Smooth Particle Mesh Ewald Method. *J. Chem. Phys.* **1995**, *103*, 8577–8593.
- (70) Boggs, P. T.; Rogers, J. E. Orthogonal Distance Regression. Statistical analysis of measurement error models and applications: proceedings of the AMS-IMS-SIAM joint summer research conference held June 10–16, 1989. 1990; pp 183–194.
- (71) Bleys, G.; Joos, P. Adsorption kinetics of bolaform surfactants at the air/water interface. *J. Phys. Chem.* **1985**, *89*, 1027–1032.
- (72) Eastoe, J.; Dalton, J. Dynamic Surface Tension and Adsorption Mechanisms of Surfactants at the Air–Water Interface. *Adv. Colloid Interface Sci.* **2000**, *85*, 103 – 144.
- (73) Swenson, H.; Stadie, N. P. Langmuir’s Theory of Adsorption: A Centennial Review. *Langmuir* **2019**, *35*, 5409–5426.
- (74) Joos, P.; Serrien, G. Adsorption Kinetics of Lower Alkanols at the Air/Water Interface: Effect of Structure Makers and Structure Breakers. *J. Colloid Interface Sci.* **1989**, *127*, 97–103.
- (75) Kirkwood, J. G.; Buff, F. P. The Statistical Mechanical Theory of Solutions. I. *J. Chem. Phys.* **1951**, *19*, 774–777.
- (76) Ben-Naim, A. Inversion of the Kirkwood–Buff Theory of Solutions: Application to the Water–Ethanol System. *J. Chem. Phys.* **1977**, *67*, 4884–4890.

- (77) Smith, P. E. Chemical Potential Derivatives and Preferential Interaction Parameters in Biological Systems from Kirkwood-Buff Theory. *Biophys. J.* **2006**, *91*, 849–856.
- (78) Bonn, D.; Eggers, J.; Indekeu, J.; Meunier, J.; Rolley, E. Wetting and Spreading. *Rev. Mod. Phys.* **2009**, *81*, 739–805.
- (79) Nijmeijer, M.; Bruin, C.; Bakker, A.; van Leeuwen, J. Wetting and Drying of an Inert Wall by a Fluid in a Molecular-Dynamics Simulation. *Phys. Rev. A* **1990**, *42*, 6052.
- (80) Ishida, N.; Kinoshita, N.; Miyahara, M.; Higashitani, K. Effects of Hydrophobizing Methods of Surfaces on the Interaction in Aqueous Solutions. *J. Colloid. Interface Sci.* **1999**, *216*, 387–393.
- (81) Schwierz, N.; Horinek, D.; Liese, S.; Pirzer, T.; Balzer, B. N.; Hugel, T.; Netz, R. R. On the Relationship Between Peptide Adsorption Resistance and Surface Contact Angle: a Combined Experimental and Simulation Single-Molecule Study. *J. Am. Chem. Soc.* **2012**, *134*, 19628–19638.
- (82) Tanford, C. Interfacial Free Energy and the Hydrophobic Effect. *Proc. Natl. Acad. Sci.* **1979**, *76*, 4175–4176.
- (83) Ashbaugh, H. S.; Pratt, L. R. Colloquium: Scaled Particle Theory and the Length Scales of Hydrophobicity. *Rev. Mod. Phys.* **2006**, *78*, 159–178.
- (84) Binks, B. P.; Johnson, A. J.; Rodrigues, J. A. Inversion of ‘Dry Water’ to Aqueous Foam on Addition of Surfactant. *Soft Matter* **2010**, *6*, 126–135.
- (85) Lucassen-Reynders, E. Contact Angles and Adsorption on Solids. *J. Phys. Chem.* **1963**, *67*, 969–972.
- (86) An, H.; Liu, G.; Craig, V. S. Wetting of Nanophases: Nanobubbles, Nanodroplets and Micropancakes on Hydrophobic Surfaces. *Adv. Colloid Interface Sci.* **2015**, *222*, 9–17.
- (87) Díaz, D.; Nickel, O.; Moraga, N.; Catalán, R. E.; Retamal, M. J.; Zelada, H.; Cisternas, M.; Meißner, R.; Huber, P.; Corrales, T. P., et al. How water wets and self-hydrophilizes nanopatterns of physisorbed hydrocarbons. *J. Colloid Interface Sci.* **2022**, *606*, 57–66.
- (88) Geyer, F.; D’Acunzi, M.; Sharifi-Aghili, A.; Saal, A.; Gao, N.; Kaltbeitzel, A.; Sloot, T.-F.; Berger, R.; Butt, H.-J.; Vollmer, D. When and How Self-Cleaning of Superhydrophobic Surfaces Works. *Sci. Adv.* **2020**, *6*, eaaw9727.
- (89) Uematsu, Y.; Bonthuis, D. J.; Netz, R. R. Impurity effects at hydrophobic surfaces. *Curr. Opin. Electrochem.* **2019**, *13*, 166–173.

Supporting Information:

Tuning contact angles of aqueous droplets on hydrophilic and hydrophobic surfaces by surfactants

Fabio Staniscia, Horacio V. Guzman, and Matej Kanduč*

Department of Theoretical Physics, Jožef Stefan Institute, SI-1000 Ljubljana, Slovenia

E-mail: matej.kanduc@ijs.si

S-1. SIMULATIONS OF BULK PROPERTIES OF THE SOLUTIONS

To calculate the bulk properties necessary for the Kirkwood–Buff theory used in sec. 3.1, we simulate three independent realizations of a homogeneous system in a cubic simulation box of edge 5 nm in the NPT ensemble for 100 ns for each concentration of surfactant. From the simulations, we extract the radial density functions g_{mw} and g_{mm} , shown in Fig. S-1, and use them in eq. (5) to calculate \mathcal{G}_{mw} and \mathcal{G}_{mm} . The latter quantities are shown in Fig. S-2 as a function of the surfactant concentration. Both \mathcal{G}_{mw} and \mathcal{G}_{mm} are independent of the concentration at low concentrations (within the numerical uncertainty), which justifies our approximation.

S-2. ADSORPTION AT A SURFACE

In Figs. S-4, S-5, and S-6, we show the comparison between MD simulations results and Langmuir (2) and Henry (3) isotherms for the values of θ not shown in Fig. 6. The parameters of the Langmuir isotherm, Γ_∞ and k_c , have been fitted, while the coefficient K_s for Henry’s law has been obtained from the fit of the Langmuir isotherm as $K = \Gamma_\infty k_c$. The outcome of these fits is shown in Figs. 7 and S-7.

S-3. ESTIMATING SURFACTANT ADSORPTION AT THE SOLID–VAPOR INTERFACE

To check that there is no adsorption at the solid–vapor interface, we run simulations of a cylindrical surfactant-containing water droplet on the solid surface. The surface has the same features as in the main simulations, except that the size along the y direction is twice as large. The droplet is periodically replicated along the x direction, as shown in Fig. S-8.

Averaging the densities over time and the x direction, we obtain the yz -resolved surfactant density profile, which is shown in Fig. S-9. From the obtained density plots of all three surfactants, it is possible to see that the density at the solid–vapor interface remains zero, which justifies our assumption.

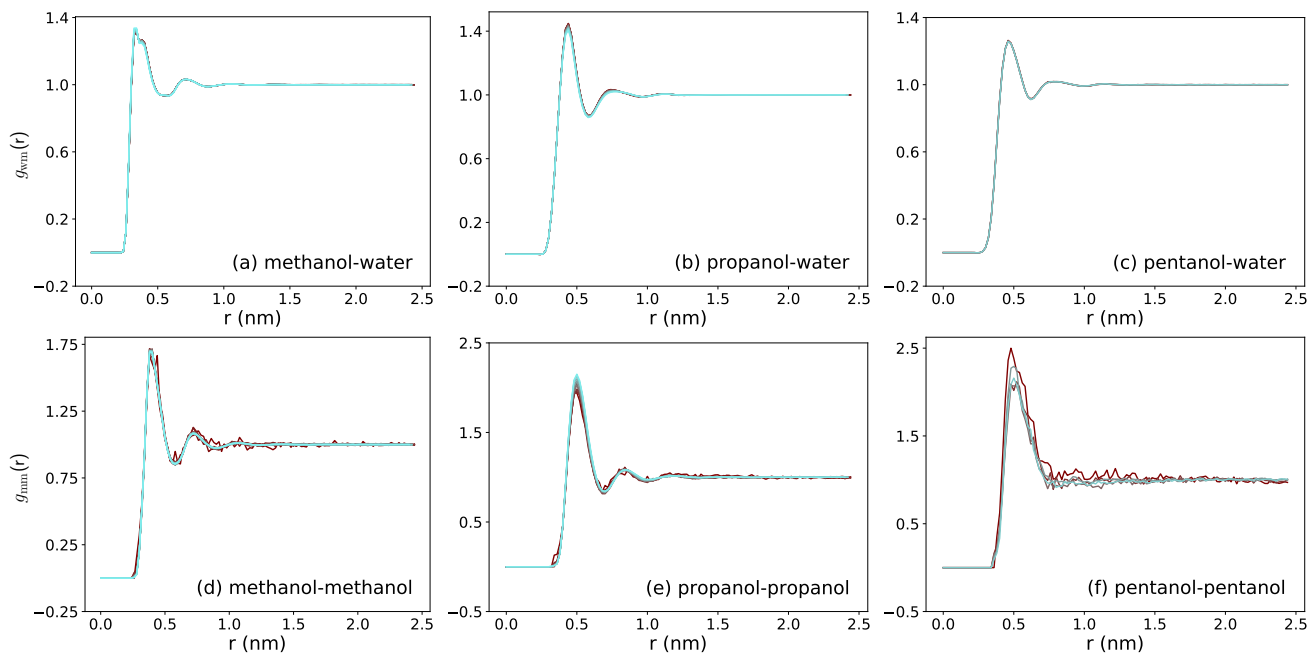


Figure S-1: Radial density functions between water and surfactant molecules (top row) and between the surfactant molecules themselves (bottom row). Different surfactant densities are shown in different colors.

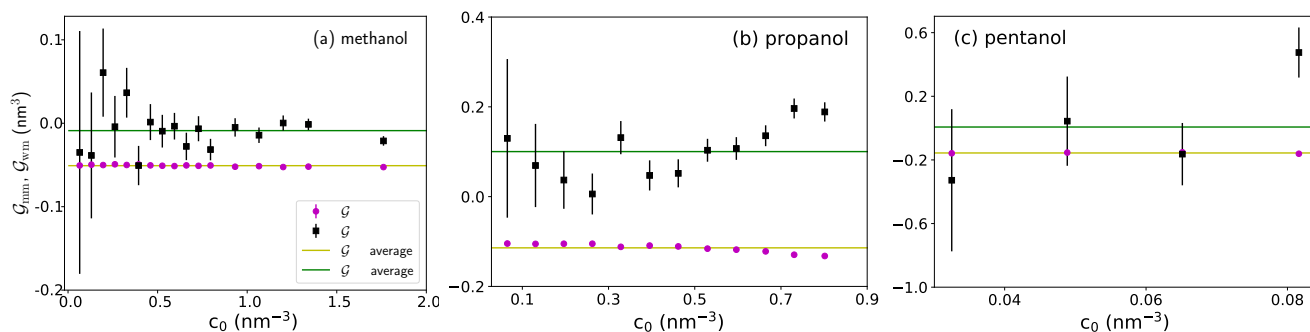


Figure S-2: Parameters \mathcal{G}_{wm} and \mathcal{G}_{mn} calculated from eq. (5) in the main text from the data in Fig. S-1 as a function of surfactant concentration. The horizontal solid lines indicate the averaged values for each data set.

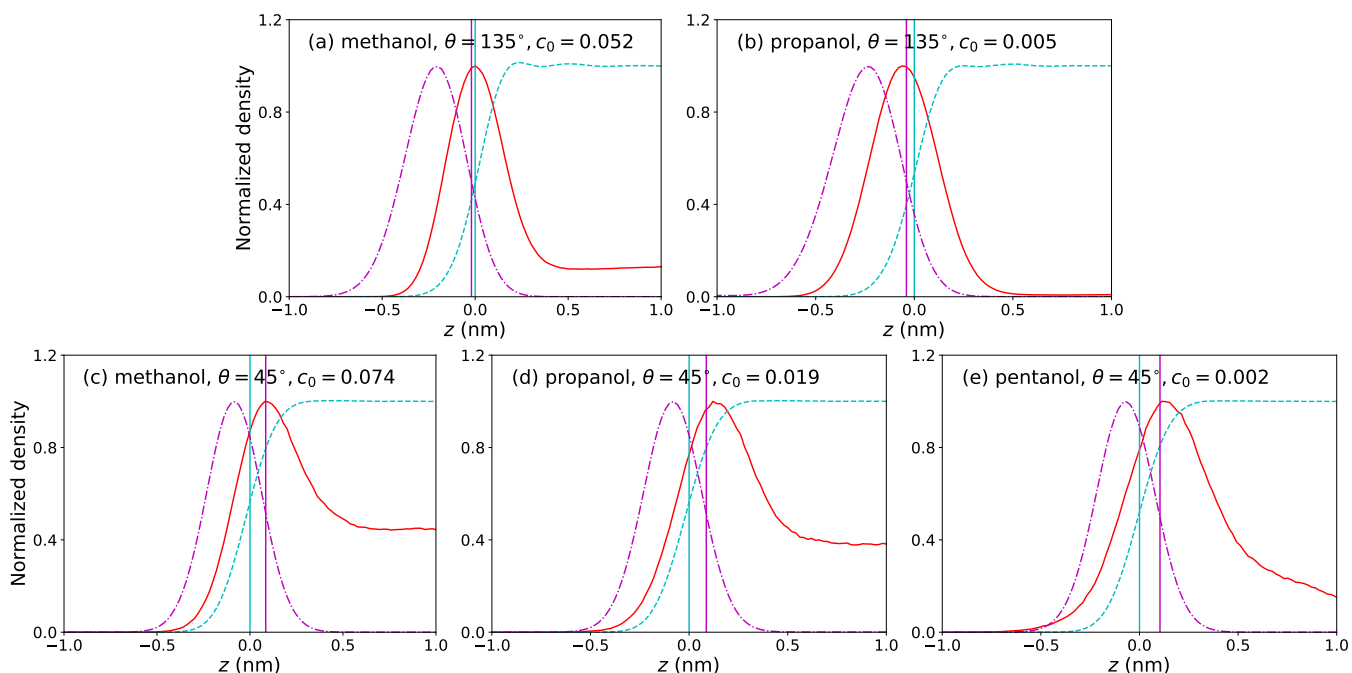


Figure S-3: Rescaled density profiles of surfactants (solid red lines), the surface OH groups (magenta dash-dotted lines), and water (cyan dashed lines). Effective phase boundaries are depicted by the Gibbs dividing surface for water (cyan) and the position at half height on the water side of the OH group (magenta).

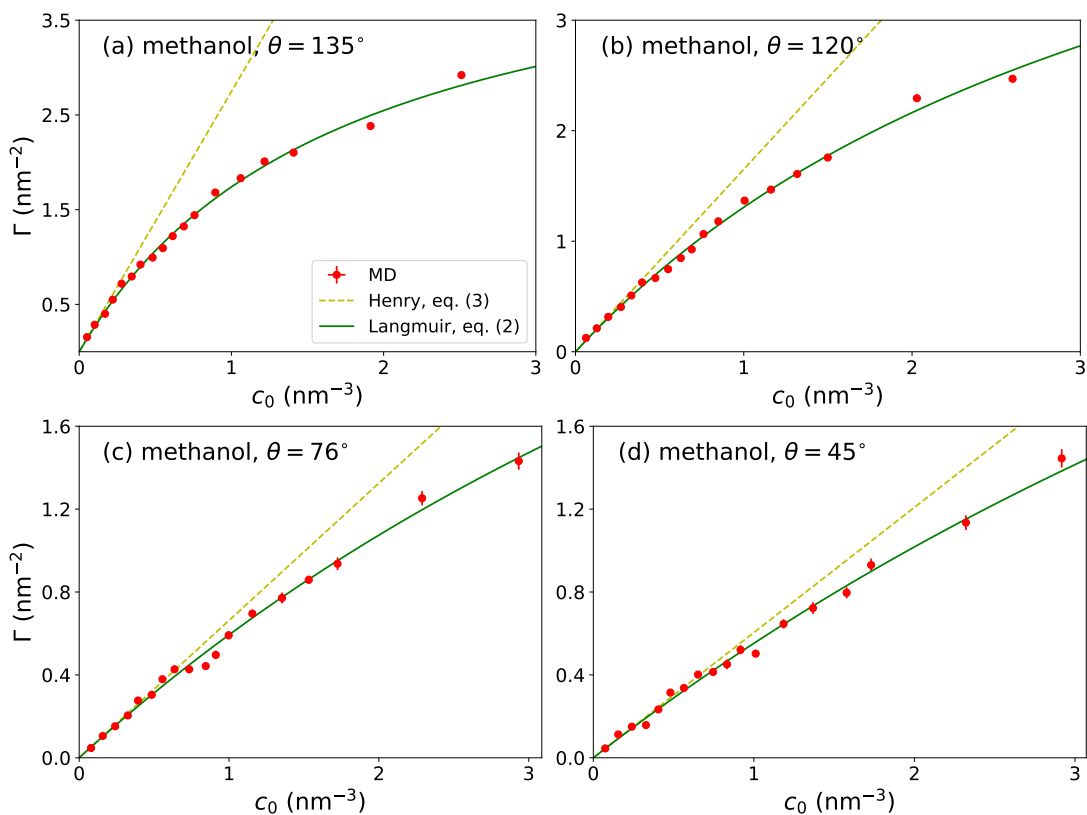


Figure S-4: Adsorption Γ at the solid-water interface as a function of surfactant concentration for various water contact angles. MD values are shown by red circles, whereas solid green lines show the fits of the Langmuir isotherm. Yellow dashed lines correspond to Henry's law (Eq. 3), for which the coefficient K_V is calculated from the Langmuir fit.

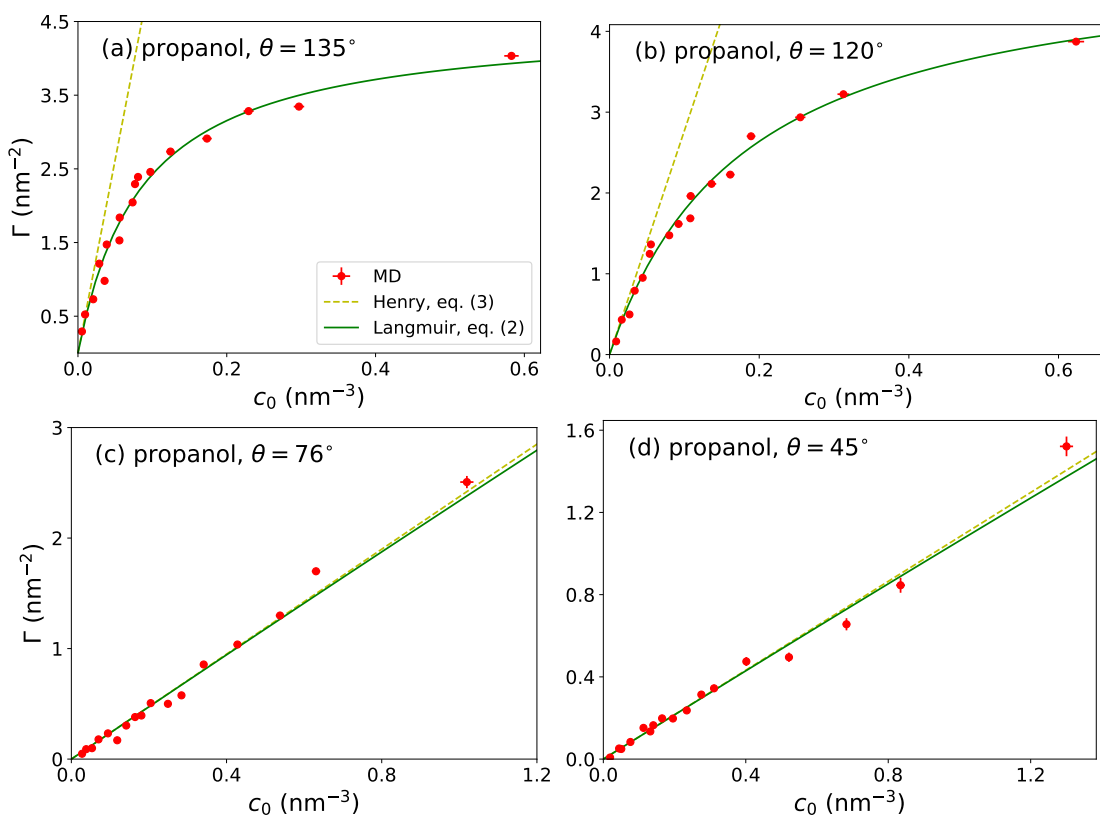


Figure S-5: Same as Fig. S-4 but for propanol.

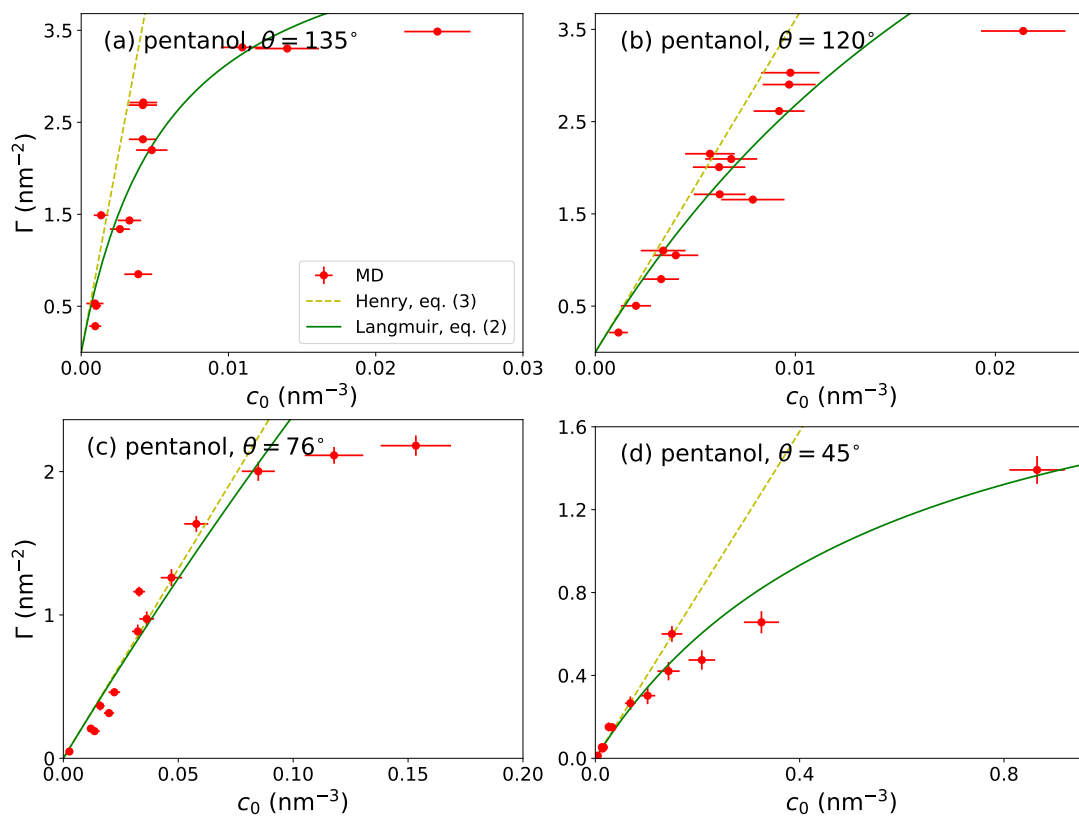


Figure S-6: Same as Fig. S-4 but for pentanol.

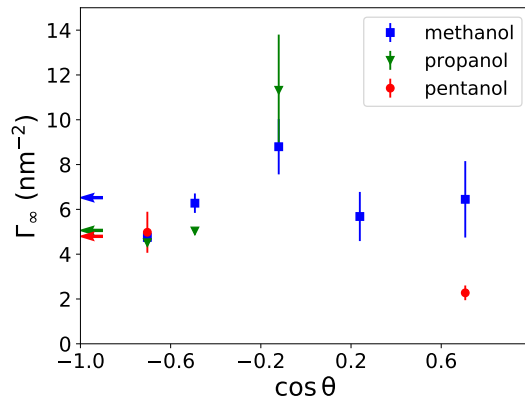


Figure S-7: The fitted saturation value Γ_{∞} from the Langmuir isotherm *versus* the surface wetting coefficient for the three different alcohols. The arrows represent Γ_{∞} for the water–vapor interface.

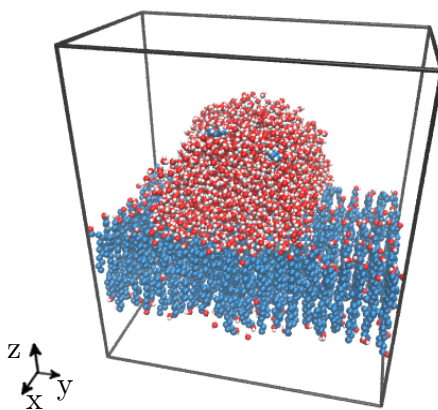


Figure S-8: Simulation snapshot of a cylindrical surfactant-containing water droplet on a planar solid surface, used to estimate the amount of the surfactant at the solid–vapor interface.

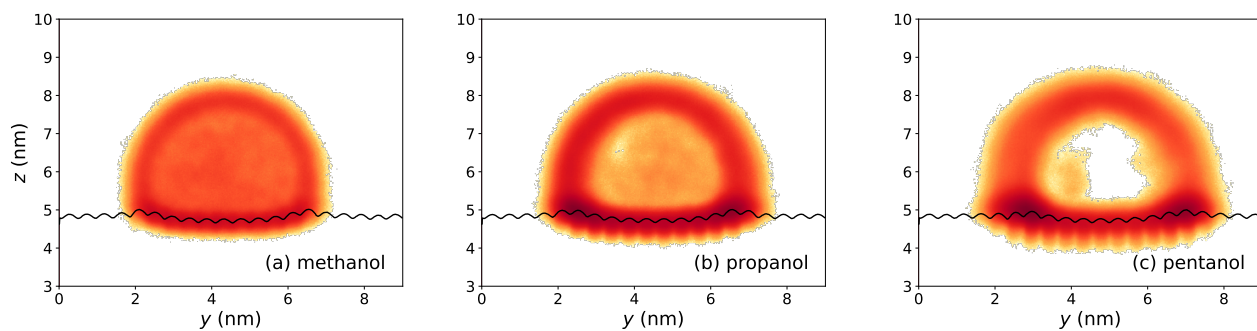


Figure S-9: Side-view surfactant density plots (in logarithmic scale) of cylindrical water droplets for (a) methanol, (b) propanol, and (c) pentanol. The color scale runs from white (low densities) to red (large densities). In all three cases, the solid surface has a contact angle of $\theta = 120^\circ$. The black lines are the dividing surfaces of the OH groups of the surface.